Applied Physics A (2020) 126:620
https://doi.org/10.1007/s00339-020-03766-1

Applied Physics A
Materials Science & Processing

Characterization of the hetero-system $ZnCo_2O_4$/ZnO prepared by sol gel: application to the degradation of Ponceau 4R under solar light

G. Rekhila[1] · A. Saidani[1] · F. Hocine[1] · S. Habi Ben Hariz[1] · M. Trari[1]

Received: 24 March 2020 / Accepted: 26 June 2020 / Published online: 18 July 2020

Abstract
Ponceau 4R is successfully oxidized on the hetero-system $ZnCo_2O_4$/ZnO under the solar light. The spinel with a nano-morphology is elaborated by the sol gel method at ~ 850 °C. The X-ray diffraction pattern exhibits narrow peak characteristics that reveals a good crystallization. The capacitance^{-2}–potential (C^{-2}–E) plot of the semiconductor $ZnCo_2O_4$ indicates p type behavior from which a flat band potential of + 0.30 V_{SCE} is determined. The energy band diagram, built from the physic-chemical properties, clearly predicts the electron transfer from the conduction band of $ZnCo_2O_4$ toward dissolved oxygen via ZnO. Indeed, the $ZnCo_2O_4$/ZnO composite improves the photocatalytic performance, where the colloidal photochemical hetero-system is successfully used for the light induced Ponceau 4R oxidation. The spinel dose and Ponceau 4R concentration are optimized. The conversion rate is controlled by UV–Visible spectrophotometry and, under the ideal conditions, the oxidation of 70% of Ponceau 4R (15 ppm) is obtained in aerated solution for less than 4 h when exposed to the solar light. The oxidation obeys a first order kinetic with a half-photocatalytic life of 130 min ($k \sim 52 \times 10^{-4}$ min^{-1}).

Keywords Ponceau 4R · Hetero-system $ZnCo_2O_4$/ZnO · Photocatalytic degradation · Kinetic · Solar light

1 Introduction

The water contaminated by heavy metals, dyes drugs and pesticides are traditionally treated by biological and/or physical methods which decreases the pollution level, but not enough to reach the limit required by the World Health Organization (WHO) [1–4]. Indeed, the classical techniques are expensive and inefficient at low concentrations (10–150 mg L^{-1}). Respectively, the advanced oxidation process (PDO) is a promising alternative for the treatment of effluent water from different industries [5–7] and the batch-process solar decontamination is found to be an effective treatment for the potable water. In this regard, the semiconductor/liquid junction, assimilated to a photo-electrochemical system to remediate the aquatic pollution [8–10]. Among the oxides, the spinels MM'_2O_4, where M and M' are commonly 3d metals, start to gain a growing popularity in photocatalysis owing to their chemical stability, non-toxicity, easy synthesis and absorption over a wide range of the solar spectrum [11, 12]. The potential of their conduction bands (~ − 1 V) [13] is below the $O_2/O_2^{\cdot}$couple, leading to spontaneous oxidation of organic molecules [14, 15]. They were used in the hydrogen production from water [16, 17] and heavy metals reduction to element states [18] under visible light illumination.

With a band gap of ~ 2 eV, the spinels absorb ~ 40% of the sunlight. The optical transition in the visible region is of d–d type, and the crystal field splitting which lifts the degeneracy of 3d orbital in a lower t_{2g} and upper e_g levels, leading to inhibited dissolution in aqueous medium [19, 20]. Moreover, the potential of the valence band (VB) and conduction band (CB) does not vary with pH and it can be suitably located with respect to redox levels in solution by a judicious selection of pH.

We tried to apply systematically the hetero-system $ZnCo_2O_4$/ZnO for the dyes degradation. Indeed, dyes are of widespread use in many industries and are commonly encountered in effluents and surface water.

The aim of the present work is to report the preparation of the spinel $ZnCo_2O_4$ by sol gel route and its

✉ G. Rekhila
rekhilagharib@gmail.com

✉ M. Trari
mtrari@usthb.dz

[1] Laboratory of Storage and Valorization of Renewable Energies, Faculty of Chemistry (USTHB), BP 32 16111, Algiers, Algeria

photo-electrochemical characterization. As possible application, the photocatalytic performance is tested toward the oxidation of Ponceau 4R, a recalcitrant molecule, upon solar light on the hetero-system $ZnCo_2O_4$/ZnO. The activity is dependent on some parameters like the sensitizer dose and dye concentration. The dye elimination was followed by UV–Visible spectrophotometry and the conversion rate reached high values under the solar light. ZnO serves to mediate the electrons transfer to adsorbed dye molecules.

2 Experimental

$ZnCo_2O_4$ was prepared by the sol gel method; the detailed procedure was reported elsewhere [21]. Briefly, stoichiometric amounts of $Zn(NO_3)_2{\cdot}6H_2O$ (Merck, 99.5%) and $Co(NO_3)_3{\cdot}9H_2O$ (Merck, 99.5%) were dissolved in water containing the gelling agent (Agar–Agar, Flucka 1 g L^{-1}). The solution was heated at 70 °C and the gel was dehydrated at 130 °C. Finally, the sample was homogenized in an agate mortar and heated at 850 °C in a programmed muffle furnace.

ZnO nanoparticles were synthetized by dissolution of $Zn(NO_3)_2{\cdot}6H_2O$ in 100 mL NaOH solution (1 M) containing 1 g of agar–agar; the solution was treated at 80 °C (1 h) and the precipitate was thoroughly washed and treated at 350 °C.

The phase composition was identified by X-ray diffraction (XRD) in the 2θ range (15°–90°) using a Siemens diffractometer (Model D-5000). The FTIR analysis was made by dispersing the spinel (~2%) in KBr (spectroscopic quality). The scanning electron microscope (SEM) image was taken with a Hitachi microscope (Model S2500). The diffuse reflectance data were collected in the range (190–900 nm) using a Specord 200 Plus spectrophotometer.

The electrical conductivity (σ) was determined by the two-probe technique with a direct current source. The thermoelectric power was measured on dense pellets sintered at 900 °C with the use of home-made equipment.

The electrical contact, performed with silver cement on sintered pellet, was automatically verified. The pellet was introduced in a glass tube and isolate by hardening araldite. The electrochemical study was done in Na_2SO_4 (0.1 M) solution using a Pyrex cell containing the working electrode, Pt as auxiliary electrode and SCE as a reference. A PGZ 301 potentiostat was used to plot the current–potential J (E) characteristics in the dark and under visible irradiation. The capacitance–potential curve (C^{-2} vs. E) was plotted at 10 kHz; the electrochemical impedance spectroscopy (EIS) data were collected on a Z_{imag} vs. Z_{real} diagram; the equivalent electrical circuit was modeled by using the Z-View software 3.4.

The photoactivity was tested through the oxidation of Ponceau 4R, a hazardous dye. The tests were carried out in a batch Pyrex reactor equipped with a cooling system whose temperature was regulated at 25 °C. The tests were realized at natural pH using 200 mL of Ponceau 4R solution at different concentrations (5–20 mg L^{-1}) with a variable spinel dose ($Y\% = x/(x+125)\times 100$, x being the mass of $ZnCo_2O_4$ while the mass of ZnO was maintained constant (125 mg). Before irradiation, the mixture was sonicated for 2 min to disperse the catalyst powder. They were kept in the obscurity for 1 h under magnetic agitation (200 rpm) to reach the absorption equilibrium. The system was exposed to solar light (95 mW cm^{-2}), the intensity of which was measured with a flux meter (Testo 545).

Aliquots (0.5 mL) of the solution were regularly withdrawn and filtered to separate the solid particles. The remaining Ponceau 4R concentration was analyzed by UV–Vis spectrophotometry (Shimadzu UV 1800). The photo catalytic efficiency was determined from the relation:

$$\eta = 100\left(C_o - C_t\right)/C_o, \tag{1}$$

where C_o and C_t are, respectively, the initial concentration and the concentration after irradiation for time (t). It is worthwhile to mention that Ponceau 4R was not oxidized by photolysis. All solutions were prepared with CO_2 free distilled water.

3 Results and discussion

The recorded XRD patterns are shown in Fig. 1. The single-phase $ZnCo_2O_4$ crystallizes in a cubic symmetry (space group Fd3m) and all XRD peaks (Fig. 1a) belong to the normal spinel $Zn[Co_2]O_4$ with a lattice constant of 0.8068 nm in agreement with the JCPDS cards No 11-1110. The structure is formed by a close packed lattice of O^{2-} ions where the octahedral cavities are occupied by Co^{3+}, while Zn^{2+} are located in tetrahedral sites. The XRD pattern of ZnO (Fig. 1b) shows a single-phase crystallizing in the hexagonal Wurtzite structure with lattice constants: $a = 0.3237$ and $c = 0.5194$ nm.

The crystallite sizes are evaluated from the broadening (β, radian) of the strongest XRD peak ($L = 0.9\,\lambda\,(\beta\cos\theta)^{-1}$). The values L (= 30 nm, $ZnCo_2O_4$ and 29 nm, ZnO) indicates that the crystallites are agglomerated, thus forming grains. Assuming spherical compact crystallites, the L value gives active surface area $\{Ssp = 6\,(d\text{exp}\,L)^{-1}\}$ equal to 30 $m^2\,g^{-1}$ for $ZnCo_2O_4$, $d$exp being the experimental density. The SEM micrographs recorded for the $ZnCo_2O_4$ sample are shown in Fig. 2. As can be seen, the sample contains fine-spherical shaped grains with an average diameter lying between 0.7 and 1.7 µm and such values confirm the agglomeration of fine crystallites.

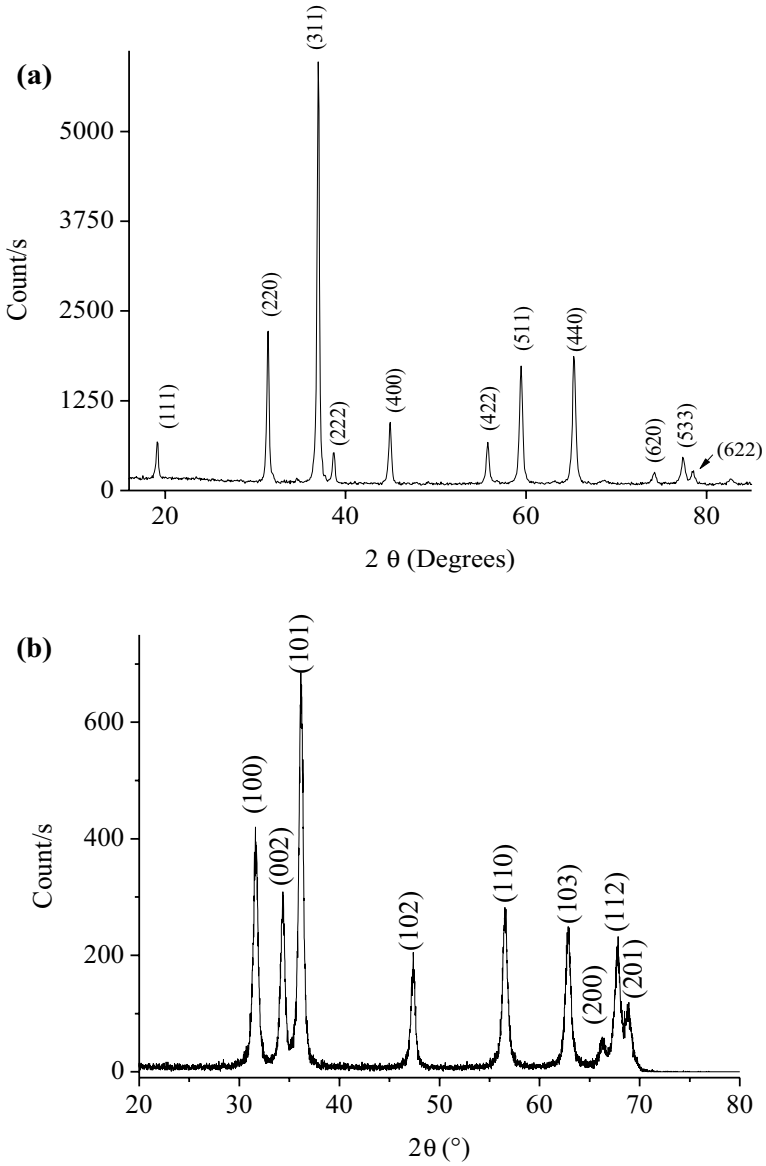

Fig. 1 XRD patterns of **a** $ZnCo_2O_4$ and **b** ZnO

The optical properties of $ZnCo_2O_4$ are typical of insulators [22] and consequently not different from other spinels [23, 24]. The incident energy ($h\nu$, eV) and absorption coefficient (α, cm^{-1}) are related by the following relation:

$$(\alpha h\nu)^n = \text{Constant} \times \left(h\nu - E_g\right), \quad (2)$$

where the parameter n depends on the transition type: $n = ½$ and 2, respectively, for indirect and direct transitions [25–27]. The intersection of the linear plot $(\alpha h\nu)^2$ with the abscissa axis indicates direct allowed a transition with E_g value of 1.82 eV (Fig. 3).

The key factor of a photocatalyst in the solar energy conversion is its semiconductor properties and the transport properties were measured for this purpose. The electron/hole (e^-/h^+) pairs are separated by the interfacial electric field (see below). The space charge region (δ) is a characteristic of classical semiconductor (Fig. 4). The low carrier density (N_A) leads to an extended width δ of in agreement with the low electrical conductivity of $ZnCo_2O_4$ ($\sigma_{300K} \sim 10^{-6}\ \Omega^{-1}\ cm^{-1}$). The conductivity $\sigma(T)$ follows an exponential law with activation energy of 0.10 eV. Such value is supported by the positive thermo-power (+500 µV K^{-1} at 300 K) which indicates that the majority carriers are holes with a concentration of the order of magnitude ~ 10^{18} cm^{-3} (Fig. 4, inset).

Ponceau 4R is a weak electrolyte and the intensity–potential J (E) curve (Fig. 5) of $ZnCo_2O_4$ electrode is plotted in neutral electrolytic salt (Na_2SO_4, pH ~ 7). The curve exhibits a plateau region down to 0.4 V with a dark current less than 0.1 mA cm^{-2}, and the behavior is similar to that of chemical diode. The wave centered at − 0.35 V is assigned to

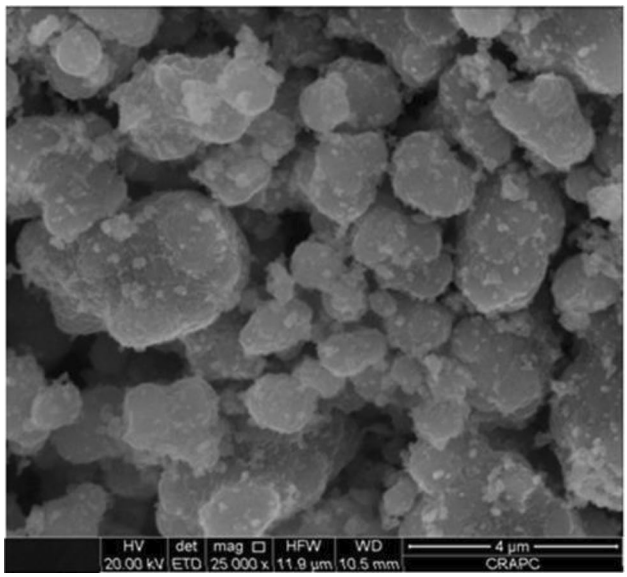

Fig. 2 SEM analysis of the spinel $ZnCo_2O_4$ prepared by sol gel route

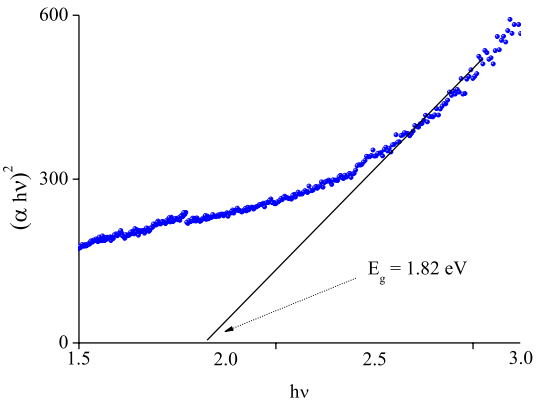

Fig. 3 Direct optical transition of the spinel $ZnCo_2O_4$

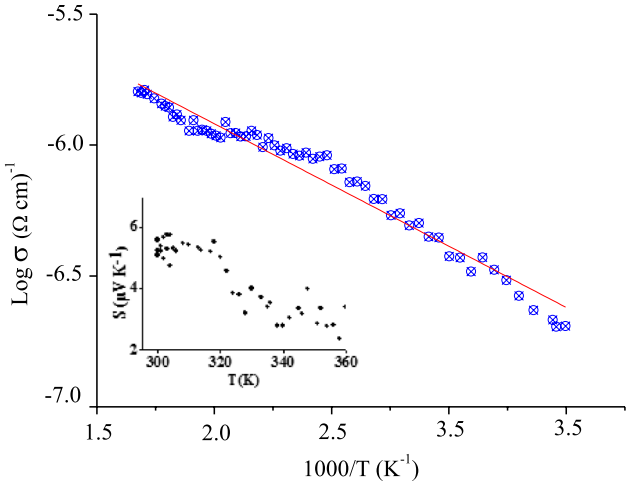

Fig. 4 The logarithm of the electrical conductivity as function of 10^3/T for$ZnCo_2O_4$. Insert: Thermal dependence of the thermo-power

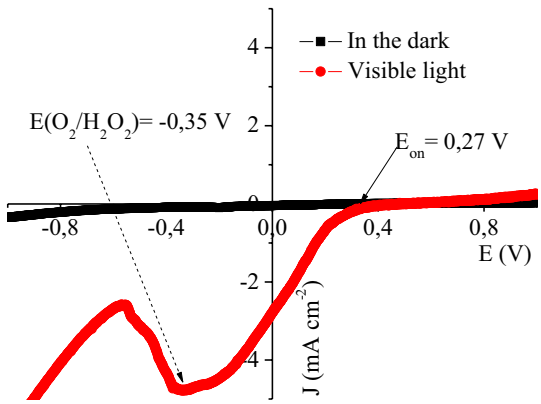

Fig. 5 The intensity–potential J (E) characteristics of $ZnCo_2O_4$ plotted in Na_2SO_4 (0.1 M) solution in the dark and under visible light illumination

the peroxide formation ($H_2O + 0.5\ O_2 + e^- \rightarrow H_2O_2$). The current decrease below − 0.6 V without reaching a plateau, is due to the H_2 evolution as evidenced by gas bubbles on the electrode. In addition, $ZnCo_2O_4$ is known to produce hydrogen under visible light [22, 28].

The photocurrent (J_{ph}) starts to flow at ~ 0.3 V (photocurrent onset potential E_{on}) and augments along the negative potentials, thus supporting the p-type conduction where the hole are the majority carriers. The flat band potential (E_{fb}) under the operating conditions is reliably determined from the capacity (C)–potential (E) relation:

$$\frac{1}{C^2} = \left(\frac{2}{\varepsilon\varepsilon_o e N_A}\right)(E_{fb} - E), \tag{3}$$

where ε (= 300) is the permittivity of the spinel, ε_o is the permittivity of vacuum, e is the electron charge and N_A is the hole concentration. The extrapolation of the fitted line at infinite capacity ($C^{-2} = 0$, Fig. 6) and the slope give the potential E_{fb} (− 0.30 V) and concentration ($N_A = 2.4 \times 10^{16}$ cm^{-3}), respectively. The flat region above − 0.2 V is ascribed to the accumulation zone with an increased recombination rate of (e^-/h^+) pairs, whereas the bending below − 0.7 V is due the maximal band bending with a zero recombination rate of (e^-/h^+) pairs. The low N_A value leads to a large depletion region ($\delta \sim 400$ nm) which is greater than the penetration depth (α_λ^{-1}), the latter is dependent on the wavelength λ. The potentials of the valence band (VB) and conduction band (CB) of $ZnCo_2O_4$ of are of high importance in photocatalysis, and the following relations compute them:

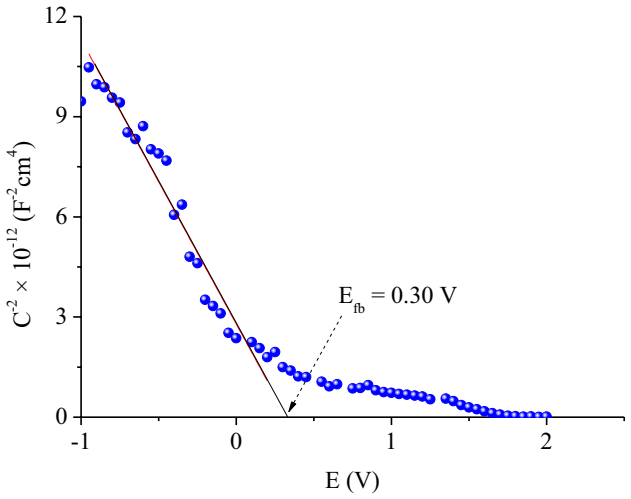

Fig. 6 The Mott–Schottky plot of *p*-type $ZnCo_2O_4$in Na_2SO_4 (0.1 M) solution

$$E_{CB} = 4.75 + e\,E_{fb} + 0.056(pH - pH_{pzc}) + E_a \quad (4)$$

$$E_{VB} = E_{CB} + E_g \quad (5)$$

(pH_{pzc} = 7.44) of ZnO determined from the drift method (Fig. 7). The values of CB (− 3.33 eV/− 1.42 V) and VB (− 5.15 eV/0.40 V) indicate that both bands made up of 3*d* orbital ($t_{2g} - e_g$) which takes then origin from the crystal field splitting of Co^{3+} in sixfold coordination.

3.1 Photocatalysis

The alternatives for the water treatment continue to attract a growing interest owing to of the large-scale pollution and the photocatalysis remains attractive in the third world not only for the protection of the environment but also for the high solar potential like Algeria with a solar constant

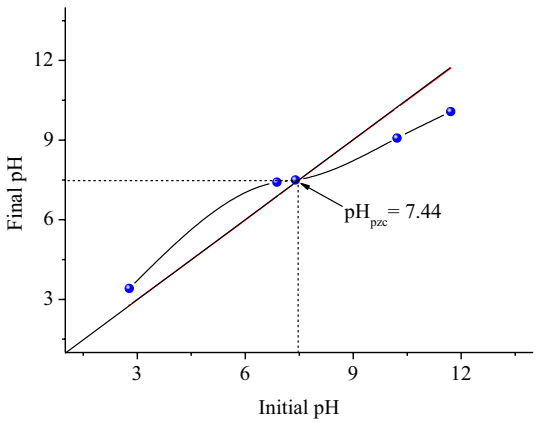

Fig. 7 Determination of the point zero charge (pH_{pzc}) of $ZnCo_2O_4$

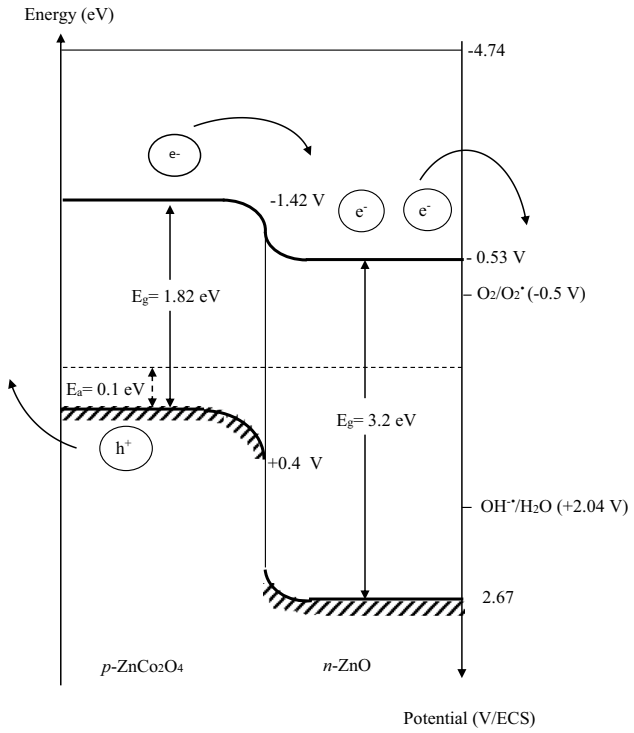

Fig. 8 Energy diagram of $ZnCo_2O_4$ in electrochemical scale at pH ~ 7

of ~ 1 kW cm^{-2}. On the other hand, the adsorption is widely used for the removal of organic molecules but remains just a transfer of the pollution and the adsorbent must be regenerated that requires a further investment. In contrast, the photocatalysis permits the water decontamination (oxidation/mineralization) [29, 30] and the advanced oxidation processes (AOPs) need reactive radicals $O_2^{\cdot}$and/or ·OH formed in the conduction and valence bands, respectively, which destroy the organic matter in the presence of dissolved oxygen [31].

Individually, the spinel and ZnO give moderate oxidation for Ponceau 4R under the solar light, respectively, 14 and 26%. However, both SCs which have different energy levels enable us to reach high conversion yields by synergy. This performance was predicted from the energy diagram of the hetero-system $ZnCo_2O_4$/ZnO_2/Ponceau 4 R solution (Fig. 8), plotted on the basis of the physic-chemical properties (E_g, E_a and E_{fb}). Generally, the radicals are generated on wide band gap semiconductors, exceeding 3 eV illuminated by the UV_A light of the sun [30, 32]. The injection of charge carriers occurs iso-energetically and the large difference ($E_{O_2/O_2^{\cdot}} - E_{CB}$) inhibits the electrons transfer, thus yielding a weak photocatalytic ability, thus yielding a weak photoactivity. Therefore, ZnO is used as an electron bridge in order to mediate the electrons transfer in solution.

$ZnCo_2O_4$-CB, formed of e_g orbital is pH independent while ZnO-VB varies by − 0.059 V pH^{-1}, this property has

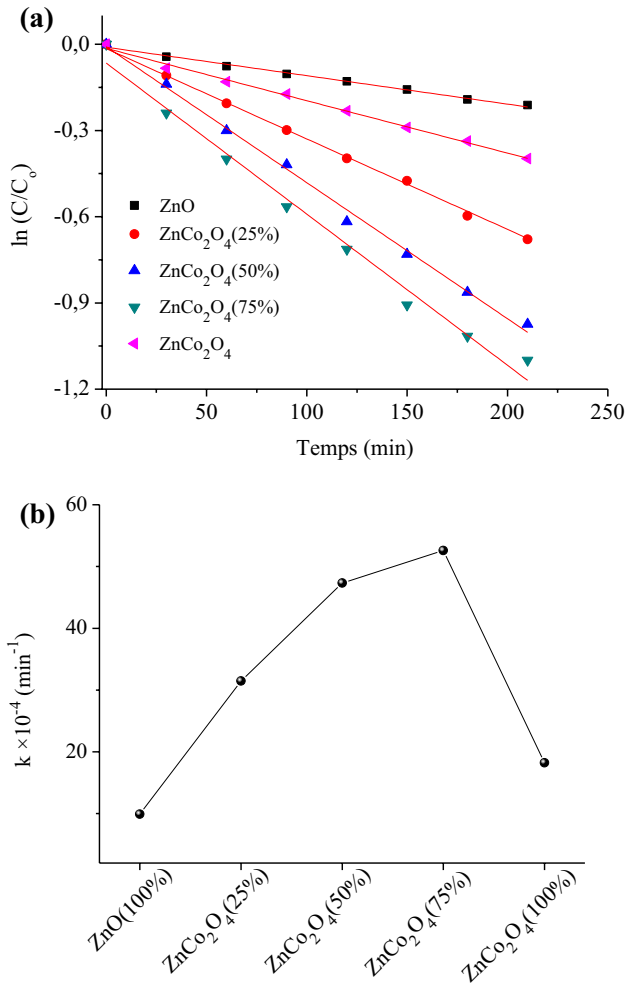

Fig. 9 **a** Dependences of ln(C/C_o) on time for different $ZnCo_2O_4$/ZnO compositions. **b** The reaction rate as a function of the $ZnCo_2O_4$/ZnO mass ratio

been exploited to get an optimal band bending at the solid interface $ZnCo_2O_4$/ZnO at pH ~ 7. On the other hand, the photocatalysis is dependent on the particle morphology and the effect of the crystallite dimension decrease on the dye mineralization is investigated. The charge carrier lifetime must be as long as possible to reach the interface. The nano-sizes are desirable in such a case and the sol gel process is suitable for elaborating powders and enhancing the surface-to-volume ratio. In addition, the porosity of $ZnCo_2O_4$ decreases the over-voltages of the electrochemical reactions and, therefore, increases the number of photoelectrochemical sites. The dark adsorption is a preamble for the photocatalysis of organic compounds. The point pH_{pzc} of ZnO, at which the adsorption occurs, is found to be 7.44 [33] and the surface is positively charged at neutral pH. The mesomeric effect of the Ponceau 4R structure occurs between the double bond and the lone pair of nitrogen and is likely responsible

Table 1 Kinetics parameters for Ponceau 4R photodecoloration

Système catalytique	k (min^{-1}) × 10^{-4}	$t_{1/2}$(min) = 0.693/k
$ZnCo_2O_4$(Y%)/ZnO		
x = 0	10	693
x = 25	31	223
x = 50	47	147
x = 75	52	130
x = 100	18	385

of binding which favors its access to catalytic sites of ZnO by electrostatic attraction.

Ponceau 4R is not degraded by photolysis while only 5% is adsorbed, as shown by the concentration measurement before and after maintaining the mixture ($ZnCo_2O_4$/ZnO) in Ponceau 4R solution for 12 h in the dark. Accordingly, the concentration decrease is mostly due to a photocatalytic mechanism adopted in the dyes degradation [34]:

$$O_{2\,ads} + e^- \rightarrow O_2^{\cdot} + H^+ \rightarrow HO_2^{\cdot} + H^+ \rightarrow H_2O_2(+e^-) \rightarrow OH^{\cdot} + OH^- \quad (6)$$

The irradiation time is fixed at 220 min. and the main parameters influencing the photocatalytic process are the catalyst dose and Ponceau 4R concentration. As expected, the performance increases with augmenting the amount of the sensitizer $ZnCo_2O_4$ (Fig. 9a) due to larger reception surface and high number of photoelectrochemical sites for visible photons with an increased generation of (e^-/h^+) pairs. The linear dependence of the photocatalytic degradation indicates a pseudo first-order kinetic:

$$\mathrm{Ln}\ C_t = -kt + \ln C_o. \quad (7)$$

The half-photocatalytic life ($t_{1/2}$), the time required to oxidize half of initial quantity of Ponceau 4R, is found to be dependent on the concentration (Table 1). The spinel dose Y% (= $x/(x+100)\times 100$ varies in the range (0–100%) while the ZnO quantity is fixed at 100 mg. The optimal dose (Y % $ZnCo_2O_4$/ZnO) under artificial illumination is found to be 75% for the Ponceau 4R oxidation (15 ppm) with a half-life of 130 min (Fig. 9b). The decline of the photoactivity above the threshold value is induced by light obstruction due to the shadowing and scattering effects of the catalyst powder in solution.

Beyond 200 min, the slope decreases progressively that is followed by gradual cessation. This tendency to saturation indicates that the layers already adsorbed are first degraded and the kinetic is controlled by the Ponceau 4R diffusion to photo-catalytic sites of the catalyst surface where the superoxides $O_2^{\cdot}$ are formed for a new desorption/photooxidation cycle. The photocatalytic process needs contact by collision which favors the electronic exchange between $ZnCo_2O_4$ and

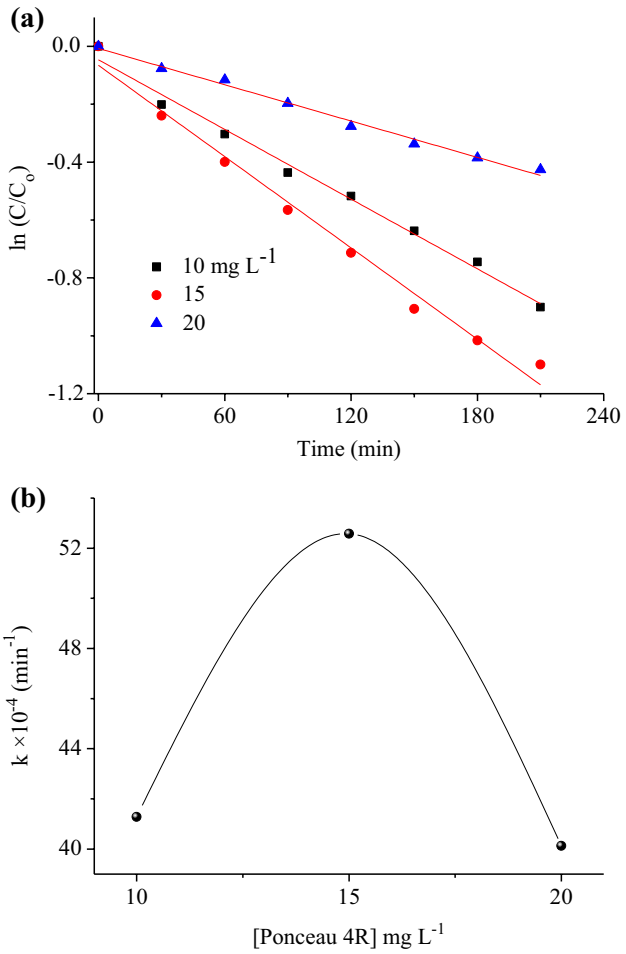

Fig. 10 **a** Effect of the initial Ponceau 4R concentration (C_o) toward the photoefficiency of the $ZnCo_2O_4$(75%)/ZnO. **b** The reaction rate as a function of the initial Ponceau 4R concentration

ZnO. The improvement in photoactivity under sunlight is due to the additional excitation of ZnO by the UV_A part of the sun, which represents about 5% of the solar flux. The effect of the initial concentration of Ponceau 4R (C_o) on the photo-degradation rate is shown in Fig. 10. At high Ponceau 4R concentration, the oxidation decreases because of the reduced light penetration (for 50 ppm, 72.69%). The degradation rate reaches a maximum due to the occupancy of all photocatalytic by the dye molecules that leads to a regression of the photoactivity [35]. Conversely, for diluted solutions, the conversion rate is augmented with decreasing C_o.

4 Conclusion

Ponceau 4R, a dye widely used in the cosmetic industry, was successfully oxidized on the hetero-system $ZnCo_2O_4$/ZnO under the solar light. The $ZnCo_2O_4$ spinel was synthesized by the sol gel method and the X-ray diffraction showed narrow peaks revealing good crystallization. The voltammetry indicated an excellent electrochemical stability with a small dark current. The capacitance of $ZnCo_2O_4$, the ratio of the variation in electric charge of the electrode to the corresponding change in the electric potential, measured in neutral medium indicates *p* type behavior. The combined optical/photo-electrochemical properties enabled us to draw the energy band diagram. The latter showed the electron transfer from the conduction of the spinel to dissolved oxygen via ZnO, predicting a high degradation, as confirmed by the experimental tests. The rate of the Ponceau 4R elimination was controlled by UV–Visible spectrophotometry and both the spinel dose and dye concentration were optimized. The photoactivity was improved upon sunlight because of the activation of ZnO by the UV photons. A conversion rate of 70% was obtained in aerated solution (Ponceau 4R, 15 ppm) within 220 min and the oxidation follows the pseudo first-order kinetic with a half-photocatalytic life of 135 min.

Acknowledgements We acknowledge the financial support from the Thematic Research Agency for Science and Technology (ATRST) of Algeria, through the national research program (PM 01/2019, CNEPRU Project No B002014N160420190001).

Compliance with ethical standards

Conflict of interest The authors declare that they have no conflict of interest.

References

1. N. Haddadou, N. Bensemma, G. Rekhila, M. Trari, K. Taïbi, Lead-free Ba application to amoxicillin photodegradation. J. Photochem. Photobiol. A Chem. Photoelectrochem. Investig. **358**, 294–299 (2018). https://doi.org/10.1016/j.jphotochem.2018.03.033
2. Z. Hammache, A. Soukeur, S. Omeiri, B. Bellal, M. Trari, Physical and photo-electrochemical properties of $MgFe_2O_4$ prepared by sol gel route: application to the photodegradation of methylene blue. J. Mater. Sci. Mater. Electron. **30**, 5375–5382 (2019). https://doi.org/10.1007/s10854-019-00830-2
3. A.M. Sevim, Synthesis and characterization of Zn and Co monocarboxy-phthalocyanines and investigation of their photocatalytic efficiency as TiO_2 composites. J. Organomet. Chem. **832**, 18–26 (2017). https://doi.org/10.1016/j.jorganchem.2017.01.011
4. D. Zhang, Y. Yin, Y. Li, Y. Cai, J. Liu, Critical role of natural organic matter in photodegradation of methylmercury in water: molecular weight and interactive effects with other environmental factors. Sci. Total Environ. **578**, 535–541 (2017). https://doi.org/10.1016/j.scitotenv.2016.10.222
5. A. Nezamzadeh-Ejhieh, S. Khorsandi, Photocatalytic degradation of 4-nitrophenol with ZnO supported nano-clinoptilolite zeolite. J. Ind. Eng. Chem. **20**, 937–946 (2014). https://doi.org/10.1016/j.jiec.2013.06.026
6. O. Ouagagui, G. Rekhila, R. Nedjar, M. Trari, Synthesis, physical and photoelectrochemical characterizations of $Sr0.5Nb_3O_8{\cdot}1.7H_2O$: application to the Rhodamine B oxidation under solar light. J. Mater. Sci. Mater. Electron. **31**, 1257–1264 (2020). https://doi.org/10.1007/s10854-019-02637-7

7. A. Mills, N. Wells, C. O'Rourke, Correlation between the photocatalysed oxidation of methylene blue in solution and the reduction of resazurin in a photocatalyst activity indicator ink (Rz Paii). J. Photochem. Photobiol. A **330**, 86–89 (2016). https://doi.org/10.1016/j.jphotochem.2016.07.020
8. M. Bingham, A. Mills, Photonic efficiency and selectivity study of M (M = Pt, Pd, Au and Ag)/TiO_2 photocatalysts for methanol reforming in the gas phase. J. Photochem. Photobiol. A Chem. (2020). https://doi.org/10.1016/j.jphotochem.2019.112257
9. Z. Boukhemikhem, R. Brahimi, G. Rekhila, G. Fortas, L. Boudjellal, M. Trari, The photocatalytic hydrogen formation and NO_2^- oxidation on the hetero-junction Ag/$NiFe_2O_4$ prepared by chemical route. Renew. Energy **145**, 2615–2620 (2020). https://doi.org/10.1016/j.renene.2019.08.021
10. S. Douafer, H. Lahmar, M. Benamira, G. Rekhila, M. Trari, Physical and photoelectrochemical properties of the spinel $LiMn_2O_4$ and its application in photocatalysis. J. Phys. Chem. Solids **118**, 62–67 (2018). https://doi.org/10.1016/j.jpcs.2018.02.053
11. I. Sebai, N. Salhi, G. Rekhila, M. Trari, Visible light induced H_2 evolution on the spinel $NiAl_2O_4$ prepared by nitrate route. Int. J. Hydrogen Energy **42**, 26652–26658 (2017). https://doi.org/10.1016/j.ijhydene.2017.09.092
12. M. Zangiabadi, A. Saljooqi, T. Shamspur, A. Mostafavi, Evaluation of GO nanosheets decorated by $CuFe_2O_4$ and CdS nanoparticles as photocatalyst for the degradation of dinoseb and imidacloprid pesticides. Ceram. Int. **46**, 6124–6128 (2020). https://doi.org/10.1016/j.ceramint.2019.11.076
13. G. Rekhila, Y. Bessekhouad, M. Trari, Hydrogen evolution under visible light over the solid solution $NiFe_{2-x}Mn_xO_4$ prepared by sol gel. Int. J. Hydrogen Energy **40**, 12611–12618 (2015). https://doi.org/10.1016/j.ijhydene.2015.07.109
14. Y. Roumila, K. Abdmeziem, G. Rekhila, M. Trari, Semiconducting properties of hydrothermally synthesized libethenite application to orange G photodegradation. Mater. Sci. Semiconduct. Process. (2016). https://doi.org/10.1016/j.mssp.2015.10.018
15. G. Zhou, J. Guo, G. Zhou, X. Wan, H. Shi, Photodegradation of orange II using waste paper sludge-derived heterogeneous catalyst in the presence of oxalate under ultraviolet light emitting diode irradiation. J. Environ. Sci. (China) **47**, 63–70 (2016). https://doi.org/10.1016/j.jes.2015.11.030
16. H. Abid, G. Rekhila, F.A. Ihaddadene, Y. Bessekhouad, M. Trari, Direct hydrogen evolution under visible light illumination on the solid solution $Cd_xZn_{1-x}S$ prepared by ultrasound-assisted route. Int. J. Hydrogen Energy **4**, 4–11 (2019)
17. U. Caudillo-Flores, M.J. Muñoz-Batista, M. Fernández-García, A. Kubacka, Bimetallic Pt–Pd co-catalyst Nb-doped TiO_2 materials for H_2 photo-production under UV and Visible light illumination. Appl. Catal. B **238**, 533–545 (2018). https://doi.org/10.1016/j.apcatb.2018.07.047
18. G. Rekhila, R. Brahimi, Y. Bessekhouad, M. Trari, Physical and photoelectrochemical characterizations of the pyrochlore $La1.9Ba0.1Sn_2O_7$: application to chromate reduction under solar light. J. Photochem. Photobiol. A Chem. **332**, 345–350 (2017). https://doi.org/10.1016/j.jphotochem.2016.08.023
19. G. Rekhila, Y. Bessekhouad, M. Trari, Synthesis and characterization of the spinel $ZnFe_2O_4$, application to the chromate reduction under visible light. Environ. Technol. Innov. **5**, 127–135 (2016). https://doi.org/10.1016/j.eti.2016.01.007
20. W. Ketir, G. Rekhila, M. Trari, A. Amrane, Vopor-polymerization strategy to carbon-rich holey few-layer carbon nitride nanosheets with large domain size for superior photocatalytic hydrogen evolution. J. Environ. Sci. (China) **24**, 2173–2179 (2012). https://doi.org/10.1016/S1001-0742(11)61043-7
21. G. Rekhila, Y. Bessekhouad, M. Trari, Visible light hydrogen production on the novel ferrite $NiFe_2O_4$. Int. J. Hydrogen Energy (2013). https://doi.org/10.1016/j.ijhydene.2013.03.087
22. G. Rekhila, Y. Gabes, Y. Bessekhouad, M. Trari, Hydrogen production under visible illumination on the spinel $NiMn_2O_4$ prepared by sol gel. Sol. Energy **166**, 220–225 (2018). https://doi.org/10.1016/j.solener.2018.02.064
23. K. Shetty, L. Renuka, H.P. Nagaswarupa, H. Nagabhushana, Direct ICNANO 2016 morphology, impedance and photocatalytic studies. Mater. Today Proc. **4**, 11806–11815 (2017). https://doi.org/10.1016/j.matpr.2017.09.098
24. K. Shetty, L. Renuka, H.P. Nagaswarupa, H. Nagabhushana, K.S. Anantharaju, D. Rangappa et al., A comparative study on $CuFe_2O_4$, $ZnFe_2O_4$ and $NiFe_2O_4$: morphology, impedance and photocatalytic studies. Mater. Today Proc. **4**, 11806–11815 (2017). https://doi.org/10.1016/j.matpr.2017.09.098
25. V.V. Atuchin, A.K. Subanakov, A.S. Aleksandrovsky, B.G. Bazarov, J.G. Bazarova, S.G. Dorzhieva, Exploration of structural, thermal, vibrational and spectroscopic properties of new noncentrosymmetric double borate Rb3NdB6O12. Adv. Powder Technol. **28**, 1309–1315 (2017)
26. V.V. Atuchin, L.I. Isaenko, V.G. Kesler, Z.S. Lin, M.S. Molokeev, A.P. Yelisseyev et al., Anion ordering, optical properties and electronic structure in K3WO3F3 elpasolite. J. Solid State Chem. Explor. **187**, 159–164 (2012). https://doi.org/10.1016/j.jssc.2011.12.037
27. A.H. Reshak, Z.A. Alahmed, J. Bila, V.V. Atuchin, B.G. Bazarov, O. Dorzhitsyrenovna et al., Exploration of the electronic structure of monoclinic α-Eu 2 (MoO_4) 3: DFT-based study and X-ray photoelectron spectroscopy. J. Phys. Chem. (2016). https://doi.org/10.1021/acs.jpcc.6b01489
28. M.S. Yancheshmeh, O.A. Sahraei, M. Aissaoui, M.C. Iliuta, A novel synthesis of $NiAl_2O_4$ spinel from a Ni–Al mixed-metal alkoxide as a highly efficient catalyst for hydrogen production by glycerol steam reforming. Appl. Catal. B Environ. (2020). https://doi.org/10.1016/j.apcatb.2019.118535
29. H. Gong, W. Chu, K. Xu, X. Xia, H. Gong, Y. Tan et al., Efficient degradation, mineralization and toxicity reduction of sulfamethoxazole under photo-activation of peroxymonosulfate by ferrate (VI). Chem. Eng. J. (2020). https://doi.org/10.1016/j.cej.2020.124084
30. P.L. de Oliveira, N.S. Lima, A.C.F. de Melo Costa, E.B. Cavalcanti, Conrado L. de Sousa, Obtaining TiO_2:$CoFe_2O_4$ nanocatalyst by Pechini method for diuron degradation and mineralization. Ceram. Int. (2019). https://doi.org/10.1016/j.ceramint.2019.12.203
31. N. Bensemma, G. Rekhila, N. Boutal, K. Taãbi, M. Trari, Photoelectrochemical properties of lead-free ferroelectric ceramic $Ba(Ti0.96Mg0.013Nb0.026)O_3$: application to solar conversion of eosin. J. Mater. Sci. Mater. Electron. **27**, 6757–6765 (2016). https://doi.org/10.1007/s10854-016-4625-z
32. B. Gomez-Ruiz, P. Ribao, N. Diban, M.J. Rivero, I. Ortiz, A. Urtiaga, Photocatalytic degradation and mineralization of perfluorooctanoic acid (PFOA) using a composite TiO_2–rGO catalyst. J. Hazard. Mater. **344**, 950–957 (2018). https://doi.org/10.1016/j.jhazmat.2017.11.048
33. K. Dib, R. Brahimi, M. Trari, Y. Bessekhouad, Optical properties of S_xZnO and their effect toward the photoacativity. Optik **178**, 1102–1110 (2019). https://doi.org/10.1016/j.ijleo.2018.10.101
34. N. Helaïli, Y. Bessekhouad, A. Bouguelia, M. Trari, *p*-Cu2O/*n*-ZnO heterojunction applied to visible light Orange II degradation. Sol. Energy **84**, 1187–1192 (2010). https://doi.org/10.1016/j.solener.2010.03.024
35. N. Helaïli, Y. Bessekhouad, A. Bouguelia, M. Trari, Visible light degradation of orange II using *x*CuyOz/TiO_2 heterojunctions. J. Hazard. Mater. **168**, 484–492 (2009). https://doi.org/10.1016/j.jhazmat.2009.02.066